Available online at www.sciencedirect.com
ScienceDirect
Journal of Computational Physics 225 (2007) 1125–1136
JOURNAL OF COMPUTATIONAL PHYSICS
www.elsevier.com/locate/jcp

A stochastic boundary forcing for dissipative particle dynamics

Adrian M. Altenhoff [a], Jens H. Walther [a,b], Petros Koumoutsakos [a,*]

[a] *Institute of Computational Science, ETH Zurich, Switzerland*
[b] *Department of Mechanical Engineering, Fluid Mechanics, Building 403, DK-2800 Lyngby, Denmark*

Received 10 September 2006; received in revised form 14 January 2007; accepted 18 January 2007
Available online 30 January 2007

Abstract

The method of dissipative particle dynamics (DPD) is an effective, coarse grained model of the hydrodynamics of complex fluids. DPD simulations of wall-bounded flows are however often associated with spurious fluctuations of the fluid properties near the wall.

We present a novel stochastic boundary forcing for DPD simulations of wall-bounded flows, based on the identification of fluctuations in simulations of the corresponding homogeneous system at equilibrium. The present method is shown to enforce accurately the no-slip boundary condition, while minimizing spurious fluctuations of material properties, in a number of benchmark problems.
© 2007 Elsevier Inc. All rights reserved.

Keywords: Dissipative particle dynamics; Boundary conditions; Wall potential; No-slip

1. Introduction

Dissipative particle dynamics (DPD) is a mesoscopic hydrodynamic model of complex flows [1]. The model amounts to solving Newton's equations for the particle motion with a force field that includes conservative, dissipative and random components. DPD models exhibit hydrodynamic behavior [2] as the dissipative and random components act as thermostats, the particle number and momentum are conserved and the interparticle forces are Galilean invariant and isotropic. The use of a soft-potential in the conservative forces allows for the simulation of hydrodynamic events at time scales that are orders of magnitude longer than those allowed by the hard-repulsion potentials involved in MD simulations.

DPD has been used extensively for the simulation of complex fluids in periodic domains [3,4]. The modeling of solid boundaries in the context of DPD has been addressed in the past [5] by freezing the particles that represent the solid boundaries [1], and by modifying the repulsive forces [6] or the particle density [7] near the solid walls. While these efforts introduce minimal additional algorithmic complexity to the standard DPD

* Corresponding author. Tel.: +41 411 632 5258; fax: +41 411 632 1703.
E-mail addresses: adriaal@student.ethz.ch (A.M. Altenhoff), walther@inf.ethz.ch (J.H. Walther), petros@ethz.ch (P. Koumoutsakos).

0021-9991/$ - see front matter © 2007 Elsevier Inc. All rights reserved.
doi:10.1016/j.jcp.2007.01.015

formulation, they have, to various extents, numerical artifacts such as the generation of fluctuations of the material properties in regions near the walls.

In recent years a number of efforts have introduced effective techniques that enforce the no-slip boundary condition in DPD simulations while minimizing the disturbance to the material properties. In [8], Visser et al. introduced a back-to-back placement of a parallel twin system. The method was shown to provide good results for two dimensional flows past flat geometries and curved boundaries. More recently, Pivkin and Karniadakis extended their prior work, on modifying the repulsive forces near the boundary [9], by a control mechanism that was shown to significantly minimize the density fluctuations [10]. The authors indicate that the formalism of this method is not restricted to DPD but it could remedy a similar pathology in other particle simulations. A similar approach we recently proposed in Ref. [11] for controlling the density fluctuations in molecular systems.

Indeed the presence of fluctuations of the material properties in regions that are not in the bulk of the system is widespread in particle simulations. These fluctuations may be physical, as is the case of the molecular layering observed in molecular dynamics simulations of water in the vicinity of graphite sheets and carbon nanotubes [12]. Spurious density fluctuations in particle systems may arise when the homogeneity of the particle description is disturbed as in the case of DPD particles in the vicinity of walls. This artifact has been also observed in the coupling of MD and continuum simulations [13,14]. In these simulations, non-periodic MD techniques are coupled to continuum solvers thus breaking the periodicity of the MD simulations at the molecular-continuum interface. This disruption of homogeneity results in density fluctuations and clustering of the molecules near the boundaries. A number of remedies have been proposed in continuum–MD couplings, such as reflecting boundaries [13], modified repulsive forces [15,16] and extended buffer zones [14] that are reminiscent of the schemes employed for DPD simulations. In a recent work, Werder et al. [17] proposed a novel approach, which employs wall forces measured in a separate equilibrium simulation subject to periodic boundary conditions. The method was shown to minimize drastically the density fluctuations in MD–continuum couplings for a number of benchmark problems.

In this work, we extend the boundary forcing introduced [17] to remedy the fluctuations of material properties in DPD simulations of flows with solid boundaries. The method imposes the stochastic wall force sampled from the probability distribution functions of the individual DPD force components. These distributions are measured in a separate simulation of the corresponding homogeneous system.

The paper is structured as follows: In Section 2, we briefly outline the governing equations and their computational implementation, while in Section 3 we present the enforcement of the no-slip boundary condition using the proposed force correction. In Section 4, we present results from the application of the method to a number of benchmark problems for wall-bounded DPD simulations.

2. Dissipative particle dynamics

The time evolution of DPD particles is described by Newton's equation of motion

$$\frac{\mathrm{d}\boldsymbol{r}_i}{\mathrm{d}t} = \boldsymbol{v}_i, \quad \frac{\mathrm{d}\boldsymbol{v}_i}{\mathrm{d}t} = \boldsymbol{f}_i, \tag{1}$$

where $\boldsymbol{r}_i$ and $\boldsymbol{v}_i$ denote the position and velocity of the ith particle carrying unit mass. The total force acting on a particle ($\boldsymbol{f}_i$) is composed of three pairwise additive forces: a conservative ($\boldsymbol{F}^{\mathrm{C}}_{ij}$), a dissipative ($\boldsymbol{F}^{\mathrm{D}}_{ij}$), and a stochastic force ($\boldsymbol{F}^{\mathrm{R}}_{ij}$)

$$\boldsymbol{f}_i = \sum_{j \neq i} \boldsymbol{F}^{\mathrm{C}}_{ij} + \boldsymbol{F}^{\mathrm{D}}_{ij} + \boldsymbol{F}^{\mathrm{R}}_{ij}. \tag{2}$$

All forces are truncated beyond a finite cutoff radius r_{c}, which represents the intrinsic length scale of the DPD model. The conservative force is given by a soft repulsion:

$$\boldsymbol{F}^{\mathrm{C}}_{ij} = \begin{cases} a\left(1 - \frac{r_{ij}}{r_{\mathrm{c}}}\right)\hat{\boldsymbol{r}}_{ij}, & r_{ij} < r_{\mathrm{c}}, \\ 0, & r_{ij} \geqslant r_{\mathrm{c}}. \end{cases} \tag{3}$$

where $\mathbf{r}_{ij} \equiv \mathbf{r}_i - \mathbf{r}_j$, $r_{ij} \equiv |\mathbf{r}_{ij}|$, $\hat{\mathbf{r}}_{ij} \equiv \mathbf{r}_{ij}/r_{ij}$ and a is the maximum repulsion between a pair of particles [18]. The dissipative and the stochastic forces are:

$$\boldsymbol{F}_{ij}^{\mathrm{D}} = -\gamma\omega^{\mathrm{D}}(r_{ij})(\hat{\boldsymbol{r}}_{ij}\cdot\boldsymbol{v}_{ij})\hat{\boldsymbol{r}}_{ij}, \tag{4}$$

$$\boldsymbol{F}_{ij}^{\mathrm{R}} = \sigma\omega^{\mathrm{R}}(r_{ij})\xi_{ij}\hat{\boldsymbol{r}}_{ij}, \tag{5}$$

where ω^{D} and ω^{R} are distance dependent weight functions vanishing for $r > r_{\mathrm{c}}$, $\boldsymbol{v}_{ij} = \boldsymbol{v}_i - \boldsymbol{v}_j$ is the relative velocity between the particles, σ the noise amplitude, γ the friction coefficient, and $\xi_{ij} = \xi_{ji}$ are normally distributed random numbers with zero mean and variance $1/\Delta t$, where Δt is the time step of the simulation. The magnitude of the dissipative and stochastic forces are related through the fluctuation-dissipation theorem [19]

$$\omega^{\mathrm{D}}(r) = (\omega^{\mathrm{R}}(r))^2, \quad \text{and} \quad \sigma^2 = 2\gamma k_{\mathrm{B}}T, \tag{6}$$

where T denotes the temperature of the system, and $k_{\mathrm{B}}T = \frac{1}{3}\sum|\boldsymbol{v}|^2$.

We choose the weight function

$$\omega^{\mathrm{D}}(r) = \begin{cases} \left(1 - \frac{r}{r_{\mathrm{c}}}\right)^2, & r < r_{\mathrm{c}}, \\ 0, & r \geqslant r_{\mathrm{c}}, \end{cases} \tag{7}$$

and integrate the system in time using the modified velocity-Verlet algorithm by Groot and Warren [20].

2.1. Implementation

The present DPD method has been implemented as a client application of a hybrid parallel particle-mesh (PPM) library [21] based on a generalized formulation of particle methods [22]. The short range interactions governing DPD simulations are efficiently treated using the cell and Verlet lists [23] of the library. The calculation of the stochastic force in DPD simulations (Eq. (5)) requires the generation of pseudo random numbers. To assure a reproducible sequence of these numbers for the stochastic force component we require that the random sequence is independent of the particular number of processors and of the specific domain decomposition. To achieve this goal, we employ a standard linear congruential generator (LCG) [24], but base the seed value (s_k) of the pseudo random number (P) on the particular particle pair involved in the force calculation, thus

$$\begin{aligned} s_{k+1}^i &= a s_k^i + c \pmod{2^{32}}, \\ s_{k+1}^j &= a s_k^j + c \pmod{2^{32}}, \\ P &= \mathrm{float}(s_k^i + s_k^j \pmod{2^{32}})/m + 0.5, \end{aligned} \tag{8}$$

where s_k^i and s_k^j denotes the kth seed value for the i and jth particles. The parameters of the present LCG are $m = 4294967296.0$, $a = 1664525$, and $c = 1013904223$ [24]. This approach is similar to a combined multiple recursive random number generator [25], and allows moreover separate calculations of $\boldsymbol{F}_{ij}^{\mathrm{R}}$ and $\boldsymbol{F}_{ji}^{\mathrm{R}}$.

3. Wall boundary conditions in DPD simulations

The enforcement of the no-slip boundary condition in the context of DPD requires modifications of the particle force field near the boundaries. A number of works of varying algorithmic complexity have been proposed to model solid walls in DPD. As it has been pointed out in [10] most of the schemes induce strong density perturbations. The challenge is to modify the force field of the particles so as to account for the no-slip boundary condition while not affecting the material properties of the fluid.

3.1. Hard walls

The impermeability of solid walls is ensured by bounce-back models of particles that cross the boundary. In order to impose the no-slip conditions we use the bounce-forward scheme proposed by Visser et al. [8]. The scheme was introduced to reduce the temperature depression observed for the bounce-backward scheme [8,9]

and uses specular reflection for the particle position, and inverts the particle velocity and forces cf. Fig. 1a. In order to study the properties of this scheme we place a bounce-forward wall in a periodic system, and measure the temperature profile perpendicular to the wall (Fig. 1b). We find that, contrary to a specular wall, both the bounce-backward (not shown) and the bounce-forward schemes distort the temperature of the fluid in the vicinity of the wall. Thus, the tangential components of the temperature display a slight, 2% increase, whereas the normal component remains uniform.

The confinement induced by the hard walls secures conservation of mass and energy. The presence of walls however disturbs the homogeneity of the particles that is usually ensured in a periodic system. This disturbance is manifested as fluctuations of the thermodynamic variables of the system. It has been observed [17] that conservation of energy is not sufficient to ensure non-spurious density and pressure fluctuations. The pressure (P) of the system is expressed as:

$$P = P_{\mathrm{K}} + P_{\mathrm{U}} = \rho_n k_{\mathrm{B}} T + \frac{1}{3V} \sum_i \sum_{j>i} \boldsymbol{r}_{ij} \cdot \boldsymbol{f}_{ij}, \tag{9}$$

where P_{K}, P_{U} denote the kinetic and virial pressures, ρ_n is the average number density, and V is the volume of the system. Note that in the presence of walls the kinetic pressure can be conserved. The presence of the hard walls disturbs however the virial pressure (P_{U}) of the system and results in strong density perturbations for dense fluids in the vicinity of the solid wall cf. Fig. 2.

Hence, the inter-particle forces of the DPD model need to be modified near boundaries in order to account for the correct mean pressure component and to minimize any kind of local disturbance on the density of the flow field.

3.2. Image particles

Hard wall models are often augmented with immobile "solid" or *image* particles placed in the solid region to impose the no-slip condition and to reduce the perturbations of the material properties of the fluid. The image particles are placed on a regular lattice and they are assigned a zero velocity to obtain a first order approximation of the no-slip condition. Higher order schemes are constructed by extrapolating the fluid velocity profile onto the image particles implicitly accounting for the no-slip condition. These schemes result however in a distorted virial pressure (Eq. (9)), and in persistent perturbations of the fluid cf. Fig. 2.

3.3. Wall potentials

The disturbance of the virial pressure component has been observed [17] in couplings of molecular dynamics and continuum simulations using Schwarz domain decompositions. In this scheme the homogeneity of the

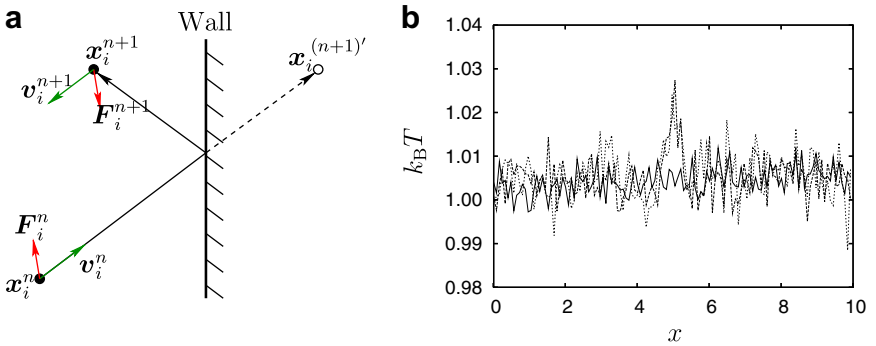


Fig. 1. Sketch of the bounce-forward reflection mechanism. (a) A particle leaving the simulation domain is reinsert using specular reflection, but with inverted velocity and force components. The bounce-forward scheme imposed at a hard wall located in the middle ($x = 5$) of a periodic system ($\rho = 3$, $a = 25$, $\sigma = 3$, $k_{\mathrm{B}}T = 1$) introduces anisotropic perturbations in the fluid temperature. (b) $k_{\mathrm{B}}T_x$ (—); $k_{\mathrm{B}}T_y$ (– –); $k_{\mathrm{B}}T_z$ (- -).

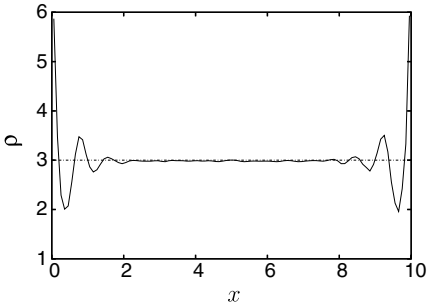


Fig. 2. Density profile obtained from DPD simulations of a Poiseuille flow [9]. The solid walls are modeled using immobile "solid" particles combined with a reflection scheme. The density perturbations of approximately 100% are observed near the walls. The dashed line shows the exact uniform density.

molecular system is disturbed when interfacing continuum cells. Werder et al. [17] modeled the modification of the virial pressure by an effective boundary force ($F_m(r)$) representing the average contribution to the virial pressure across a fictitious wall immersed in a periodic system cf. Fig. 3. Thus

$$P_{\mathrm{U}} = \rho_n \int_0^{r_c} F_m(r)\,\mathrm{d}r. \tag{10}$$

F_m can be measured directly from Eq. (9) in a separate simulations or obtained from the radial distribution function and the interparticle force [17]

$$F_m(r_{\mathrm{w}}) = -2\pi\rho_n \int_{z=r_{\mathrm{w}}}^{r_{\mathrm{c}}} \int_{x=0}^{\sqrt{r_{\mathrm{c}}^2 - z^2}} g(r) F_z(r) \frac{z}{r}\,\mathrm{d}x\,\mathrm{d}z, \tag{11}$$

where $r = \sqrt{x^2 + z^2}$, and r_{w} denotes the distance to the boundary (Fig. 3). F_z is the normal component of the interparticle force, with non-zero contributions from the conservative and dissipative forces.

3.4. Stochastic boundary forcing

The boundary forcing described in the previous subsection is extended in this work in order to take into account the fluctuations inherent to DPD systems.

We compute the probability distribution function of the different force contributions and components in a separate calculation of a homogeneous system. Fig. 4 shows the probability density functions of the force contributions for a homogeneous DPD fluid with the parameters: $\rho = 3$, $a = 25$, $\sigma = 3$, and $k_{\mathrm{B}}T = 1$, respectively. The probability density functions are measured in a periodic system using 200×100 bins to resolve the force

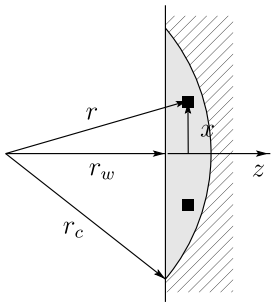


Fig. 3. Integration domains for effective boundary forces. r_{c} is the cutoff distance and r_{w} the distance to the wall. The normal force contributions along z are integrated over the shaded area using polar coordinates, the tangential force contributions along x using cartesian coordinates.

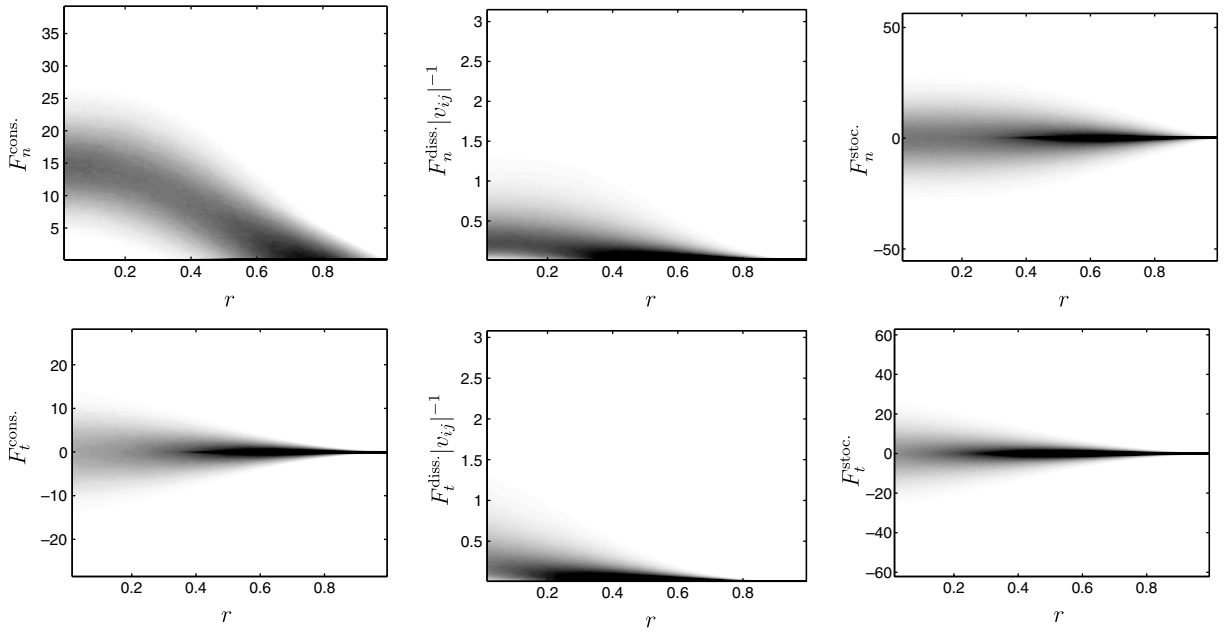


Fig. 4. Probability of the normal (top) and tangential (bottom) of the conservative, dissipative and stochastic forces (from left to right).

and distance measures. The analysis of the skewness and the kurtosis of the distributions (not shown) indicates that these distributions are in general non-Gaussian and uncorrelated in time.

The conservative and stochastic forces depend solely on the particle location (Eqs. (3) and (4)) and we model the contribution from these forces by sampling the corresponding probability distribution functions (Fig. 4) at the particular wall distance (r_w).

The dissipative force depends on both the particle position and of the relative velocity and formally requires sampling of both parameters ($r_w, \boldsymbol{v}_i$). However, in the present study we sample the normalized force ($\boldsymbol{F}^{\text{diss}}/|\boldsymbol{v}_{ij}|$) and model the velocity dependence by considering the wall as a thermal bath of particles fluctuating at $k_B T$. The mean flow of the thermal bath is assumed to vary linear from zero at $r = r_c$ to a full counter flow at $r = 0$ which result in a velocity difference of $v_{ij} \approx (2 - r_w/r_c)(\Theta - v_i)$ where Θ is a Maxwell distribution with zero mean and variance $k_B T$.

Thus we model the total wall force on the ith particle ($\boldsymbol{F}_i^{\text{W}}$) as

$$\boldsymbol{F}_i^{\text{W}}(r_w) = \begin{pmatrix} \chi_N^{\text{C}}(r_w) + \left(2 - \frac{r_w}{r_c}\right)\chi_N^{\text{D}}(r_w)(\Theta - v_{N,i}) + \chi_N^{\text{R}}(r_w) \\ \chi_T^{\text{C}}(r_w) + \left(2 - \frac{r_w}{r_c}\right)\chi_T^{\text{D}}(r_w)(\Theta - v_{T,i}) + \chi_T^{\text{R}}(r_w) \end{pmatrix}, \tag{12}$$

where χ are the probability distribution functions, measured in a separate simulation with the fluid at rest and subject to periodic boundary conditions. We note that applying the mean value of the distribution functions is equivalent to the wall potential proposed by Werder et al. [17].

4. Results

We present the results obtained using the proposed stochastic wall model applied to a number of benchmark problems. We first consider a fluid at rest confined between two parallel walls and study the perturbations introduced onto the fluid from the presence of the solid wall. We then consider the Poiseuille flow problems to demonstrate the ability of the proposed method to enforce the no-slip condition. We finally present results from simulations of the flow past an oscillating flat wall, and the flow past circular cylinders.

4.1. Fluid at rest

We consider a fluid at rest, confined between two parallel walls located at $x = 0$ and $x = 10$. A fluid density of $\rho = 3$ is obtained by placing 3000 particles inside a computational box of size $10 \times 10 \times 10$. The DPD parameters of the simulation are: $a = 25$, $\sigma = 3$, and $k_B T = 1$. The simulation is conducted for 45,000 time steps, with a time step of 0.01. Statistics are collected at every time step, starting after an initial 5000 time steps of equilibration.

For this test case we conduct two simulations: one with the full probabilistic model (Eq. (12)), and one where we only apply the mean wall force as obtained from the mean of the distribution functions (Fig. 4). The time average density profiles from the two simulations are shown in Figs. 5a and b. Both profiles display a significant reduction in the density perturbations, here 6%, compared to the perturbations of 100% previously observed in simulations without wall forces [9] cf. Fig. 2. In this test the proposed mean wall force alone (Fig. 5a) appears to be sufficient in reducing the perturbations of the fluid density. Note, however, that in the present case the lack of fluctuations in the mean flow model results in a reduced temperature at the solid walls cf. Fig. 5c. When we apply the full stochastic model we recover the correct, uniform temperature profile cf. Fig. 5d. For fluids with higher densities ($\rho > 3$), however we find an increase in the temperature at the wall (not shown). We are actively investigating methods to address this problem.

4.2. Poiseuille flow

We consider the Poiseuille flow problem in order to test the ability of the proposed model to enforce the no-slip boundary condition. The Poiseuille flow is usually understood to be driven by an externally applied pressure gradient, but for isothermal flow [26], this is equivalent to a flow driven by a body force e.g., a gravitational

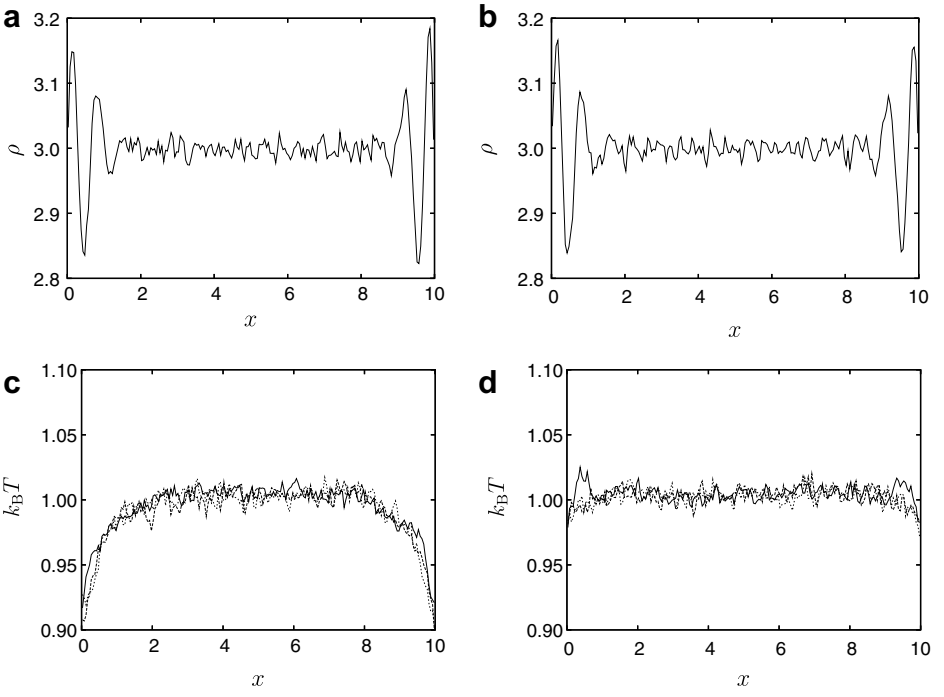


Fig. 5. DPD simulations of a fluid at rest, confined between two parallel walls. Applying the proposed mean wall force result in perturbations of the fluid density of 6% (a) and a 10% reduced fluid temperature in the vicinity of the solid walls (c). The cooling appears to be isotropic as demonstrated by the individual components of the temperature: $k_B T_x$ (—), $k_B T_y$ (– –) and $k_B T_z$ (- -). The stochastic nature of the full probabilistic model results in a similar uniform density profile (b), but provides the fluctuations require to maintain a uniform temperature profile (d).

force (mg) acting on each particle. In the simulations we place parallel walls at $x = 0$ and $x = 10$ and drive the flow by a gravitational acceleration (g_z) of 0.02. Starting from a fluid at rest, a steady flow develops with a parabolic velocity profile

$$u(x) = \frac{\rho g h^2}{8\mu}\left[\frac{x}{h} - \left(\frac{x}{h}\right)^2\right], \tag{13}$$

where μ denotes the fluid viscosity, and h the distance between the walls [27]. All the quantities are averaged for 40,000 time steps after an initial 160,000 time steps of equilibration. In Fig. 6 we show the results obtained with the parameters used in Ref. [9], thus $\rho = 3$, $a = 25$, $\sigma = 3$, and $k_B T = 1$. The results indicate that the flow does not introduce further perturbations in the fluid density and temperature, both remaining below 6% and 2%, respectively. The velocity profile is found to satisfy the no-slip condition at the boundary with a relative error of 4%. The slip was found to be insensitive to the density of the fluid (not shown).

As a second validation, we repeat the Poiseuille flow problem with the parameters used in Ref. [28], thus $\rho = 4$, $a = 18.75$, $\sigma = 3$, and $k_B T = 1$, in a computational domain of size $30.5 \times 5.0 \times 10.0$. From the simulations we obtain a maximum velocity of 8.650 and an estimated viscosity of 1.076 both within 0.2% of the values reported in Ref. [28].

4.3. Stokes flow near an oscillating flat plate

In order to demonstrate the accuracy of the proposed scheme for unsteady flows, we consider the Stokes flow near an oscillating flat plate. We conduct the simulation with the parameters used in Ref. [9] with a computational domain of size $10 \times 10 \times 10$, with solid walls located at $y = 0$ and $y = 10$, and periodic boundary conditions imposed in the x- and z-directions. The lower wall is oscillating with a velocity $U_x = \sin(\Omega t)$, with $\Omega = \pi/20$ [9]. The parameters of the fluid are: $\rho = 10$, $a = 3$, $\sigma = \sqrt{3}$, and $k_B T = \frac{1}{3}$. The kinematic viscosity is estimated according to [20]

$$\nu = \frac{45(k_B T)^2}{2\pi\rho\sigma^2 r_c^3} + \frac{\pi\sigma^2\rho r_c^5}{1575 k_B T}, \tag{14}$$

thus, here $\nu = 0.2060$.

The computational domain is divided into 20 equally sized bins in the y-direction, and the data are collected at 8 time points during the cycle, with a window of 5 time steps. The simulation is conducted for 200,000 time steps with a time step of $\delta t = 0.01$ with a total of 100 periods. The phase averaging is conducted for 50 period after an initial 50 periods of equilibration. The resulting velocity profiles are found in good agreement with the analytical solution cf. Fig. 7, with an absolute error below 1%.

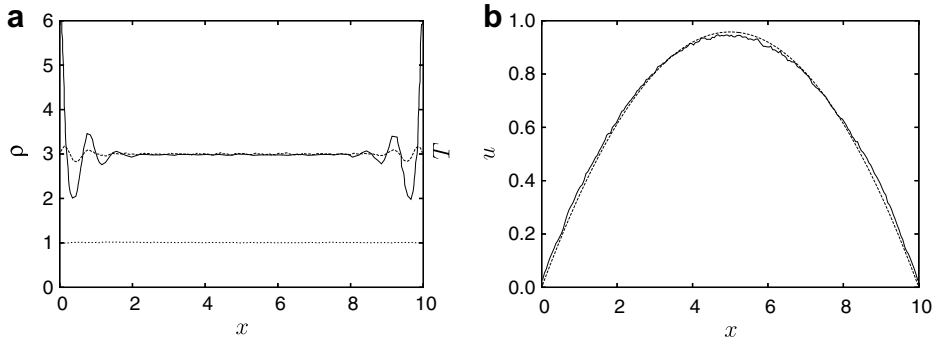


Fig. 6. DPD simulations of the Poiseuille flow problem. (a) The density (--) and temperature (···) profiles obtained using the present boundary method display a significant reduction in the perturbations compare to previous studies (—) [9]. (b) The velocity profile is found in good agreement with the Navier–Stokes solution (--).

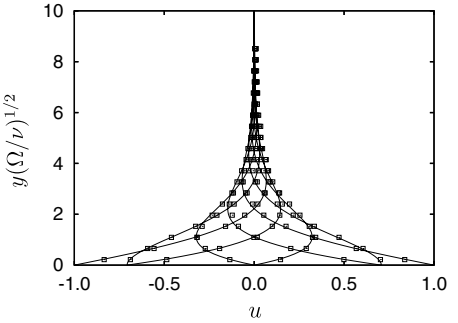


Fig. 7. Stokes flow near an oscillating flat plate: We show the velocity profiles at eight instances during the period: $t = 2k\pi/8$, $k = 0, \ldots, 7$. DPD simulations are indicated with squares, analytic solutions with lines.

4.4. Flow past a circular cylinder

The last test case involves the flow past a circular cylinder demonstrating the capability of the method to handle non-planar geometries. We choose the parameters recently considered in similar DPD simulations [29], with Reynolds numbers ($Re = UD/\nu$) of 10, 20, 30 and 40, where D is the diameter of the cylinder and U the onset flow speed. The flow is imposed by reassigning a random velocity to the particles in the inlet region [29] ($L_i = 2r_c$) located at the left boundary cf. Fig. 8. The random velocity is drawn from a Maxwellian distribution with mean values of $(U, 0, 0)$. Otherwise, periodic boundary conditions are imposed in all spatial directions. The size of the computational domain ($L_x \times L_y \times L_z$) is chosen sufficiently large to avoid excessive blockage (D/L_y) of the flow. The parameters governing the fluid are: $\rho = 4.0$, $a = 18.75$, $\sigma = 3$, and $k_B T = 1$. With these parameters the fluid viscosity is $\nu = 0.271$ (Eq. (14)) and the isothermal speed of sound (c_s) [29] is 3.05. In order to assure an effectively incompressible flow we choose flow speeds U sufficiently low to obtain Mach numbers ($Ma = U/c_s$) below $\approx$0.3 cf. Table 1.

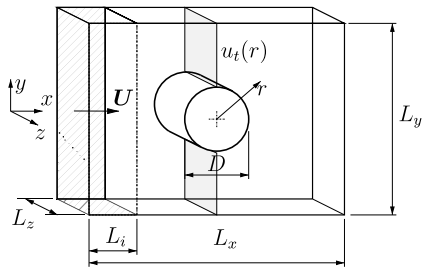


Fig. 8. DPD simulations of the flow past a circular cylinder. (a) Schematic of the simulation setup. The cylinder of diameter D is placed in the center of the computational box of size (L_x, L_y, L_z). A uniform velocity profile with mean $\boldsymbol{U} = (U, 0, 0)$ is imposed to particles in the inlet region of size L_i. Radial profiles of the tangential velocity and density are extracted in the vertical plane intersecting the center of the cylinder (shaded area).

Table 1
Simulation parameters for the flow past a circular cylinder

Re	$L_x \times L_y \times L_z$	D	D/L_y	U	Ma
10	$150 \times 150 \times 3$	5.6	3.7%	0.48	0.16
20	$150 \times 150 \times 3$	5.6	3.7%	0.98	0.32
30	$150 \times 150 \times 3$	8.0	5.3%	1.00	0.32
40	$150 \times 150 \times 3$	11.0	7.3%	1.00	0.32

The diameter (D) and onset flow speed (U) are combined with a fluid viscosity (ν) of 0.271 to attain Reynolds numbers ($Re = UD/\nu$) of 10, 20, 30, and 40, respectively. To allow comparison with incompressible fluid flow, the velocity is chosen sufficiently low to assure Mach numbers ($Ma = U/c_s$) below $\approx$0.3. c_s is the isothermal speed of sound, here $c_s = 3.05$. D/L_y is the blockage.

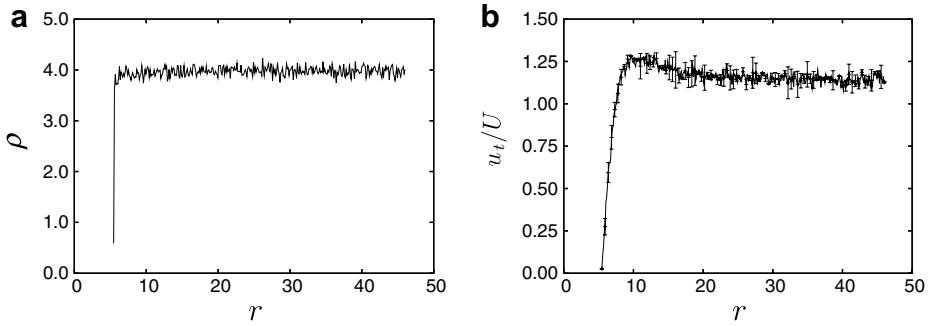


Fig. 9. DPD simulations of the flow past a circular cylinder at Re = 40. The extracted radial density profile (a) is uniform throughout the system. The corresponding tangential velocity profile (u_t/U) is found to satisfy the no-slip condition at the wall and to reach a uniform velocity $u_t/U \approx 1.14$ in the free stream. The error bars in the velocity are obtained from the measured variation in the velocity in the planes below and above the cylinder cf. Fig. 8.

The four systems are equilibrated for ca. 15,000 time steps with a time step of 0.01 corresponding to a non-dimensional equilibration time (TU/D) of ≈10. At this time the flow has reached a steady state and we sample the flow for ca. 50,000–60,000 time steps ($TU/D \approx 50$). For the simulation at a Reynolds number of 40 we extract the radial density profile along the vertical plane intersection the cylinder (Fig. 8). The profile is clearly uniform cf. Fig. 9a with negligible perturbations at the solid wall. The corresponding tangential velocity profile (Fig. 9b) is found to satisfy the no-slip condition at the solid wall and to reach a uniform velocity ($u_t/U \approx 1.14$) slightly (14%) above the onset flow speed due to the blockage of the flow. The velocity fields shown in Figs. 10a and b indicate a separated flow, which is confirmed by the fluid streamlines cf. Fig. 10c. The flow clearly displays two separation zones downstream of the cylinder.

The drag coefficient (C_D) is computed from the time average of the total wall force distributed onto the near wall particles and the change in impulse from particles bouncing the wall. The drag coefficient is found in reasonable agreement with previous simulations [29–31] and experiments [32] with maximum deviations less than 7% cf. Table 2. The periodic boundary conditions imposed in the cross stream direction (y) and the resulting blockage of the flow is expected to be responsible for the high drag values.

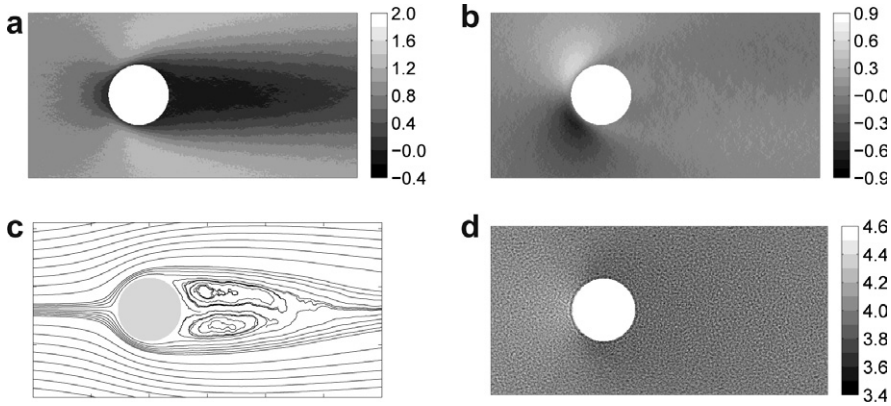


Fig. 10. DPD simulations of the flow past a circular cylinder at $Re = 40$. The steady state velocity components: (a) u and (b) v indicate that the flow is separated, which is confirmed by the streamlines shown in (c). A uniform density field (d) is observed at the solid walls, and with small variations in flow reflecting the variation in pressure.

Table 2
Drag coefficient for the flow past a circular cylinder

	$Re = 10$	$Re = 20$	$Re = 30$	$Re = 40$
Tritton [32]	2.93	2.08	1.76	1.58
Dennis and Chang [30]	2.85	2.05	–	1.52
He and Doolen [31]	3.17	2.15	–	1.50
De Palma et al. [29]	3.18	1.95	–	–
Present	2.82 ± 0.11	2.08 ± 0.03	1.82 ± 0.02	1.69 ± 0.02

5. Conclusions

We have presented a new stochastic boundary forcinzg for DPD simulations of flows with no-slip boundaries. The model is based on the construction of probability distribution functions of the DPD force components from the simulation of a homogeneous, periodic system at the same state point. These probability distributions provide information for the dynamics of the system that is being simulated and help to reduce the spurious fluctuations of the material properties in DPD simulations of wall-bounded flows. The success of this stochastic model is demonstated in exemplary flows including Poiseuille and Stokes flow over a flat plate and the flow past a circular cylinder. Present work focuses in extending this stochastic boundary forcing to hybrid molecular-continuum simulations.

Acknowledgments

We acknowledge support by the CO-ME National Center of Competence in Research of the Swiss Science Foundation (SNF). J.H.W. acknowledges partial support by Julie Damms's Studiefond.

References

[1] P.J. Hoogerbrugge, J.M.V.A. Koelman, Simulating microscopic hydrodynamics phenomena with dissipative particle dynamics, Europhys. Lett. 19 (3) (1992) 155–160.
[2] Pep Espanol, Mariano Revenga, Smoothed dissipative particle dynamics, Phys. Rev. E 67 (4) (2003) 026705-1–026705-12.
[3] Pep Español, Dissipative particle dynamics with energy conservation, Europhys. Lett. 40 (1997) 631–636.
[4] Eirik G. Flekkøy, Peter V. Coveney, From molecular dynamics to dissipative particle dynamics, Phys. Rev. Lett. 83 (9) (1999) 1775–1778.
[5] M. Revenga, I. Zúñiga, P. Espanol, Boundary conditions in dissipative particle dynamics, Comput. Phys. Commun. 121–122 (1999) 309–311.
[6] Janette L. Jones, Moti Lal, J. Noel Ruddock, Neil A. Spenley, Dynamics of a drop at a liquid/solid interface in simple shear fields: a mesoscopic simulation study, Faraday Discuss. 112 (1999) 129–142.
[7] P. Malfreyt, D.J. Tildesley, Dissipative particle dynamics simulations of grafted polymer chains between two walls, Langmuir 16 (10) (2000) 4732–4740.
[8] D.C. Visser, H.C.J. Hoefsloot, P.D. Iedema, Comprehensive boundary method for solid walls in dissipative particle dynamics, J. Comput. Phys. 205 (2005) 626–639.
[9] Igor V. Pivkin, George Em Karniadakis, A new method to impose no-slip boundary conditions in dissipative particle dynamics, J. Comput. Phys. 207 (2005) 114–128.
[10] Igor V. Pivkin, George E. Karniadakis, Coarse-graining limits in open and wall-bounded dissipative particle dynamics systems, J. Chem. Phys. 124 (2006) 184101.
[11] E.M. Kotsalis, J.H. Walther, P. Koumoutsakos, Control of density fluctuations in hybrid atomistic-continuum simulations of dense liquids, Phys. Rev. E, accepted.
[12] T. Werder, J.H. Walther, R.L. Jaffe, T. Halicioglu, P. Koumoutsakos, On the water–graphite interaction for use in MD simulations of graphite and carbon nanotubes, J. Phys. Chem. B 107 (2003) 1345–1352.
[13] Ju Li, Dongyi Liao, Sidney Yip, Coupling continuum to molecular-dynamics simulation: reflecting particle method and the field estimator, Phys. Rev. E 57 (6) (1998) 7259–7267.
[14] X.B. Nie, S.Y. Chen, W.N. E, M.O. Robbins, A continuum and molecular dynamics hybrid method for micro- and nano-fluid flow, J. Fluid Mech. 500 (2004) 55–64.
[15] Sean T. O'Connell, Peter A. Thompson, Molecular dynamics-continuum hybrid computations: a tool for studying complex fluid flow, Phys. Rev. E 52 (6) (1995) R5792–R5795.
[16] E.G. Flekkøy, G. Wagner, J. Feder, Hybrid model for combined particle and continuum dynamics, Europhys. Lett. 52 (3) (2000) 271–276.

[17] Thomas Werder, Jens H. Walther, Petros Koumoutsakos, Hybrid atomistic-continuum method for the simulation of dense fluid flows, J. Comput. Phys. 205 (2005) 373–390.
[18] Bruce M. Forrest, Ulrich W. Suter, Accelerated equilibration of polymer melts by time-coarse-graining, J. Chem. Phys. 102 (18) (1995) 7256–7266.
[19] P. Espanol, P. Warren, Statistical-mechanics of dissipative particle dynamics, Europhys. Lett. 30 (4) (1995) 191–196.
[20] Robert D. Groot, Patrick B. Warren, Dissipative particle dynamics: bridging the gap between atomistic and mesoscopic simulation, J. Chem. Phys. 107 (11) (1997) 4423–4435.
[21] I.F. Sbalzarini, J.H. Walther, M. Bergdorf, S.E. Hieber, E.M. Kotsalis, P. Koumoutsakos, PPM – a highly efficient parallel particle-mesh library for the simulation of continuum systems, J. Comput. Phys. 215 (2006) 566–588.
[22] P. Koumoutsakos, Multiscale flow simulations using particles, Annu. Rev. Fluid Mech. 37 (2005) 457–487.
[23] M.P. Allen, D.J. Tildesley, Computer Simulation of Liquids, Clarendon Press, Oxford, 1987.
[24] Donald E. Knuth, The Art of Computer Programming, Seminumerical Algorithms, second ed., Addison-Wesley, 1981.
[25] Pierre L'Ecuyer, Combined multiple recursive random number generators, Oper. Res. 44 (5) (1996) 816–822.
[26] Dino Risso, Patricio Cordero, Generalized hydrodynamics for a Poiseuille flow: theory and simulations, Phys. Rev. E 58 (1) (1998) 546–553.
[27] Ronald L. Panton, Incompressible Flow, second ed., Wiley, 1996.
[28] Xijun Fan, Nhan Phan-Thien, Ng Teng Yong, Xuhong Wu, Diao Xu, Microchannel flow of a macromolecular suspension, Phys. Fluids 15 (1) (2003) 11–21.
[29] Pietro De Palma, P. Valentini, M. Napolitano, Dissipative particle dynamics simulation of a colloidal micropump, Phys. Fluids 18 (2006) 027103.
[30] S.C.R. Dennis, G. Chang, Numerical solutions for steady flow past a circular cylinder at Reynolds numbers up to 100, J. Fluid Mech. 42 (1970) 471–489, part 3.
[31] Xiaoyi He, Gary Doolen, Lattice Boltzmann method on curvilinear coordinates system: flow around a circular cylinder, J. Comput. Phys. 134 (1997) 306–315.
[32] D.J. Tritton, Experiments on the flow past a circular cylinder at low Reynolds numbers, J. Fluid Mech. 6 (4) (1959) 547–567.